Water Resources Research

RESEARCH ARTICLE
10.1029/2022WR033387

Posterior Assessment of Parameters in a Time Domain Random Walk Model of Partitioning Tracer Tests in Two-Phase Flow Scenarios

Emanuela Bianchi Janetti[1], **Alberto Guadagnini**[1,2], **and Monica Riva**[1,2]

[1]Dipartimento di Ingegneria Civile e Ambientale (DICA), Politecnico di Milano, Milano, Italy, [2]Department of Hydrology and Atmospheric Sciences, University of Arizona, Tucson, AZ, USA

Key Points:

- A time domain random walk approach is used to model breakthrough curves of partitioning tracers observed in laboratory column experiments
- Sample distributions of model parameters constrained on experimental data are obtained through a stochastic inverse modeling technique
- Stochastic estimation of model parameters embeds uncertainty affecting concentration measurements and partition coefficient information

Supporting Information:

Supporting Information may be found in the online version of this article.

Correspondence to:

M. Riva,
monica.riva@polimi.it

Citation:

Janetti, E. B., Guadagnini, A., & Riva, M. (2023). Posterior assessment of parameters in a time domain random walk model of partitioning tracer tests in two-phase flow scenarios. *Water Resources Research*, *59*, e2022WR033387. https://doi.org/10.1029/2022WR033387

Received 2 AUG 2022
Accepted 26 APR 2023

Author Contributions:

Conceptualization: Emanuela Bianchi Janetti, Alberto Guadagnini, Monica Riva
Formal analysis: Emanuela Bianchi Janetti, Alberto Guadagnini, Monica Riva
Funding acquisition: Alberto Guadagnini, Monica Riva
Methodology: Emanuela Bianchi Janetti, Alberto Guadagnini, Monica Riva
Supervision: Alberto Guadagnini, Monica Riva
Writing – original draft: Emanuela Bianchi Janetti

Abstract We provide a reliable and efficient methodological framework for the interpretation of laboratory-scale partitioning tracer test data under uncertainty. The proposed approach rests on a Time domain random walk (TDRW) particle tracking methodology. The range of applicability of the latter is extended to include transport of partitioning tracers upon considering retardation and trapping mechanisms. A classical maximum likelihood (ML) approach is applied considering the extensive set of experimental observations of Dwarakanath et al. (1999, https://doi.org/10.1021/es990082v). This yields best estimates of model parameters, including residual immobile phase saturation, the partition coefficient and the parameters of the memory function employed to simulate the impact of solute trapping. Experimental observations of the partition coefficient are included in the objective function upon relying on a regularization term. We show that considering these types of information, which are typically obtained through batch experiments, is important to attain joint estimates of the partition coefficient and of residual immobile phase saturation. Sample probability distributions of model parameters conditional on available data are then assessed through a stochastic inverse modeling approach. This step poses a significant challenge in terms of computational effort and is performed through a reduced order surrogate model. Our results show that the TDRW-based approach can effectively capture the key features of the observed breakthrough curves of the various partitioning tracers analyzed and provide satisfactory estimates of residual immobile phase saturation.

1. Introduction

Tracers are typically employed in industrial (Dean et al., 2016; Huseby et al., 2015; Shen et al., 2017) and environmental (Solcova et al., 2022) settings to characterize attributes of subsurface systems (i.e., reservoirs/aquifer) such as, for example, permeability, porosity, or parameters driving geochemical interactions at a scale of interest. These are chemical compounds that can be added to the fluids residing in the porous formation. The analysis of their migration across the system enables one to gain enhanced knowledge about the system functioning. Passive tracers migrate within the fluid phase in which they are injected (usually water, which is taken as a wetting phase in a typical subsurface multiphase flow setting) without any interaction with formation fluids and/or geomaterials. Otherwise, a partitioning tracer is tailored to take advantage of its capability to move back and forth between wetting and non-wetting phases, the latter phase being typically oil. Due to this particular behavior, inter-well tracer tests involving injection and recovery of partitioning tracers have been performed since the 1970s to enhance our knowledge about important reservoir/aquifer characteristics (e.g., residual oil saturation and overall oil volume) that can favor optimal and sustainable use of subsurface energy resource (Allison et al., 1991; Tang, 1992). These tests are based on the simultaneous injection of several tracers, each associated with a given partition coefficient (defined as the ratio between the concentration of the tracer in the oil and in the water phase) at one or more injection wells and the subsequent monitoring of tracer concentrations at one or more observation wells. If the non-wetting phase is at residual saturation, passive (or non-partitioning) tracers remain in the wetting phase and are transported according to the velocity distribution therein. Otherwise, partitioning tracers can reach also the non-wetting phase due to diffusion processes. Therefore, partitioning tracer tests are often performed for the estimation of the residual oil saturation and volume to support enhanced oil recovery operations, eventually through unconventional approaches to increase energy production. Studies related to this technique can be found at the laboratory and field scales (see, e.g., Annable et al., 1998; Dean et al., 2016; Dwarakanath et al., 1999; Huseby et al., 2015; Jin et al., 1995, 1997, Shen et al., 2017). Laboratory scale studies are particularly critical to increase our knowledge of the underlying mechanisms. On one hand, they are key to enhance our ability to model

Writing – review & editing: Emanuela Bianchi Janetti, Alberto Guadagnini, Monica Riva

these in the presence of various sources of uncertainty that might hamper characterization of mass transport processes across natural porous media. On the other hand, the above-mentioned laboratory scale experiments are performed at the Darcy scale and the associated results cannot be transferred to different scales of interest without a proper upscaling. This is a crucial issue which is beyond the scope of the present contribution. In the above referenced studies the results of partitioning tracer tests are interpreted upon resting on models based on different types of analytical (or otherwise numerical) solutions of the advective dispersion equation (ADE) including a linear retardation term. A notable weak point of these studies is their reliance on simple analytical solutions that cannot be easily extended to interpret more complex situations arising from, for example, heterogeneous system parameters (i.e., velocity and dispersion coefficient) and/or considering three-dimensional settings. Moreover, estimates of model parameters in the above mentioned studies are typically assessed without considering uncertainty of available measurements and no information is provided about the uncertainty of the estimated parameters.

Random Walk (RW) particle tracking is an efficient and flexible Lagrangian method that is typically employed for the numerical solution of advective-dispersive transport in heterogeneous flow fields. In the RW approach the solute plume is represented by a set of noninteracting particles and solute concentration is assessed by evaluating the density distribution of these particles which migrate through the system due to advection and dispersion. Classical RW particle tracking schemes are based on the analogy between diffusion theory and stochastic processes relying on the strict equivalence between the Langevin equation, and the advection-dispersion equation (e.g., Delay et al., 2005; Kinzelbach, 1988; Salamon et al., 2006). For advection-dominated transport settings, the RW particle tracking approach is a well-established alternative for modeling subsurface transport with respect to the classical grid-based Eulerian methods that suffer from numerical diffusion. Moreover, based on the independence of each particle trajectory, the RW methodology is intrinsically adaptable to parallelization, thus yielding a significant advantage in terms of computational time. An example of a computational tool for the simulation of solute transport in groundwater systems particularly suitable for parallelization is proposed by Rizzo et al. (2019).

In some of the classical RW approaches, particles are displaced through an advective (deterministic) and a dispersive (stochastic) component. These take place at discrete time steps, with a variable spatial increment that depends on the local velocity and on the random noise associated with the dispersive component. Another approach to RW particle tracking considers a fixed spatial increment and a (variable) transition (or travel) time is evaluated for each particle and for each computational step. This approach is typically termed time domain random walk (TDRW; e.g., Banton et al., 1997; Delay et al., 2002; Dentz et al., 2012, James & Chrysikopoulos, 2001; Russian et al., 2016 and references therein). This approach is not affected by numerical dispersion if the spatial discretization, Δ, fulfills condition $\Delta < 2\,D/u$ where D and u denote the dispersion coefficient and the velocity magnitude, respectively.

In a similar context, Cvetkovic et al. (2004) and Painter et al. (2008) explicitly account for heterogeneous trapping and correlations between transport parameters including an explicit expression (inverse Gaussian) for the random advective/dispersive arrival time. Recently, Sole-Mari et al. (2020) proposed an innovative particle tracking schemes that use kernel functions to allow particle interactions.

A key objective of this study is to provide an application of the formulation of the TDRW proposed by Dentz et al. (2012) and Russian et al. (2016) to include modeling of transport of partitioning tracers across a porous medium. We mimic the retardation effect displayed by partitioning versus non-partitioning tracers upon combining the TDRW scheme with a linear retardation component and a multirate mass transfer approach (e.g., Carrera et al., 1998; Dentz & Berkowitz, 2003; Haggerty & Gorelick, 1995). The latter is a particularly convenient framework as it describes transport in the presence of immobile zones in which the solute can be immobilized/trapped for a certain amount of time. Our distinctive aims are then: (a) to present a TDRW modeling approach to characterize the behavior of partitioning tracers documented through available tests performed at the laboratory scale and (b) effectively embedding partitioning tracer data in a stochastic inverse modeling (or history matching) framework. The latter is conducive to a probabilistic characterization of model parameters conditioned on available observation of state variable (tracer concentrations) and (eventually) information on some of the model parameters (e.g., partition coefficient) obtained through other types of experiments. In contrast to a deterministic model calibration framework, our approach has the additional benefit to enable one to assess the way uncertainty associated with model parameters and concentration data propagates to target modeling goals, such as the estimate of residual oil saturation in the system, which is a critical information given by the use of partitioning

tracers. The applicability and the performance of the proposed approach and ensuing operational framework are shown in an exemplary setting based on an extensive partitioning tracer data set (Dwarakanath et al., 1999).

2. Methodology

2.1. Transport Model

We consider an experimental scenario where a partitioning and a non-partitioning tracer are simultaneously introduced at the bottom of a fully saturated column packed with a given porous medium. Tracer concentrations are measured at the outlet section (top) of the column. The system is characterized by the presence of an immobile fluid phase (e.g., oil, hereafter denoted with subscript o) trapped in the column at a given residual saturation, S_{or}, and a flowing phase (e.g., water, hereafter denoted with subscript w) at saturation $S_w = 1 - S_{or}$. Partitioning tracers tend to distribute between the mobile and immobile fluid phases. They are therefore subject to a delayed breakthrough at the column outlet with respect to the non-partitioning tracer.

We describe transport of a partitioning solute η by embedding retardation and trapping phenomena within the advection-dispersion equation, that is,

$$\frac{\partial c_{\eta,w}(\mathbf{x},t)}{\partial t} + \frac{S_{or}}{S_w}\frac{\partial c_{\eta,o}(\mathbf{x},t)}{\partial t} + F_m(\mathbf{x},t) = -\nabla\cdot\left[\mathbf{v}(\mathbf{x})c_{\eta,w}(\mathbf{x},t)\right] + \nabla\cdot\left[\underline{\underline{\mathbf{D}}}(\mathbf{x})\nabla c_{\eta,w}(\mathbf{x},t)\right], \tag{1}$$

where $c_{\eta,\alpha}$ is concentration of the partitioning tracer in fluid phase α (with $\alpha = w, o$); $\mathbf{v}(\mathbf{x})$ is the fluid (e.g., water) velocity vector; and $\underline{\underline{\mathbf{D}}}(\mathbf{x})$ is the dispersion tensor. The sink/source term F_m represents the mass of solute that is apportioned between the two (mobile and immobile) phases. Assuming equilibrium, one can introduce the partition coefficient, K_η, quantifying the affinity of η to the trapped phase, as

$$K_\eta = \frac{c_{\eta,o}}{c_{\eta,w}}. \tag{2}$$

Values of K_η are typically estimated through batch experiments. These are then used under flow-through conditions to estimate the immobile phase saturation and volume starting from partitioning tracer breakthrough curves, BTCs (see, e.g., Jin et al., 1995). Making use of Equation 2, Equation 1 can be rewritten as

$$R_\eta\frac{\partial c_{\eta,w}(\mathbf{x},t)}{\partial t} = -\nabla\cdot\left[\mathbf{v}(\mathbf{x})c_{\eta,w}(\mathbf{x},t)\right] + \nabla\cdot\left[\underline{\underline{\mathbf{D}}}(\mathbf{x})\nabla c_{\eta,w}(\mathbf{x},t)\right] - F_m; \qquad \text{with } R_\eta = 1 + K_\eta\frac{S_{or}}{S_w}, \tag{3}$$

R_η being the retardation coefficient. Various approaches have been used to describe F_m. Here, we follow Haggerty et al. (2000) and conceptualize F_m as

$$F_m = \int_0^t dt'\varphi(\mathbf{x},t')\frac{\partial}{\partial t}c_{\eta,w}(\mathbf{x},t-t'), \tag{4}$$

φ being the memory function. We solve the system of Equations 3 and 4 using a generalization of the TDRW approach (see, e.g., Carrera et al., 1998; Delay et al., 2002; Dentz et al., 2012; Haggerty & Gorelick, 1995; Russian et al., 2016). The tracer plume is discretized into N_p particles (also denoted as random walkers) whose position is updated for N_s time steps encompassing the total temporal window analyzed. Particles are injected through the system and then moved from the centroid of voxel j, $\mathbf{x}_j$, to the centroid of voxel i, $\mathbf{x}_i$, assuming that $\mathbf{x}_j$ and $\mathbf{x}_i$ are connected, according to

$$\mathbf{x}_i[t(n+1)] = \mathbf{x}_j[t(n)] + \xi_{ij}; \quad t(n+1) = t(n) + \Theta_j; \quad \Theta_j = \theta_j + \sum_{l=1}^{n_{T,j}}\vartheta_{jl} \quad \text{with } n = 1,\ldots,N_s. \tag{5}$$

Here, the total travel time, Θ_j, that a particle takes to migrate from $\mathbf{x}_j$ to $\mathbf{x}_i$ is given by the sum of (a) a transition time θ_j associated with particle displacement across the mobile phase (hereafter denoted as mobile transition time) and (b) a total trapping time related to $n_{T,j}$ trapping events, ϑ_{jl} being the duration of the l-trapping event; ξ_{ij} is a vector pointing from the centroid of voxel j to the centroid of voxel i, and only orthogonal transitions are allowed.

The probability that a particle travels from $\mathbf{x}_j$ to $\mathbf{x}_i$ is termed transition probability, w_{ij}. It is evaluated as (e.g., Dentz et al., 2012)

$$w_{ij} = \frac{b_{ij}}{\sum_{[jk]} b_{kj}} \text{ with } \sum_{ij} w_{ij} = 1 \quad \text{and} \quad b_{ij} = \frac{S_{ij}}{V_j R_\eta}\left[\frac{\hat{D}_{ij}}{|\xi_{ij}|} + \frac{|v_{ij}|}{2}\left(\frac{v_{ij}}{|v_{ij}|} + 1\right)\right], \tag{6}$$

where the notation $\sum_{[jk]}$ corresponds to the sum over all nearest neighbors of voxel i; S_{ij} denotes the contact surface between voxels i and j; V_j is the volume associated with voxel j; $\hat{D}_{ij}$ is the effective diffusion coefficient between voxels i and j (rendered through different types of formulations depending on the dimensionality of the system; e.g., Dentz et al., 2012; Noetinger & Estebenet, 2000); and v_{ij} represents the component along $\boldsymbol{\xi}_{ij}$ of velocity $\mathbf{v}_j$ evaluated at $\mathbf{x}_j$. Note that the first and second term in the formulation of b_{ij} account for diffusion and advection, respectively. Accordingly, the advective component of b_{ij} reduces to $|v_{ij}|$ when voxel j is located downstream of voxel i and vanishes otherwise (i.e., when $\mathbf{x}_j$ is upstream of $\mathbf{x}_i$).

Following Russian et al. (2016), we treat the transition time θ_j as a random variable distributed according to an exponential probability density function (p_{θ_j})

$$p_{\theta_j}(t) = \frac{w_{ij}}{b_{ij}} \exp\left(-\frac{w_{ij}}{b_{ij}} t\right). \tag{7}$$

Trapping events occur at a rate ω_j during a particle transition characterized by a mobile transition time θ_j. The latter affects the number of trapping events n_{Tj} that are drawn from the Poisson-distribution

$$p_{n_{T,j}}(n|\theta_j) = \frac{(\omega_j \theta_j)^n}{n!} \exp(-\omega_j \theta_j). \tag{8}$$

In the following, we consider a constant trapping rate (i.e., $\omega_j = \omega$) and a trapping time ϑ_{jl} distributed according to a Pareto density function

$$p_{\vartheta_{jl}}(t) = \begin{cases} \beta \dfrac{\tau^\beta}{t^{\beta+1}} & \text{if } t \geq \tau \\ 0 & \text{if } t < \tau \end{cases} \tag{9}$$

where β and τ are the shape and scale parameters of the distribution, respectively. As shown by Benson and Meerschaert (2009), the memory function in Equation 4 can be related to the trapping time density (Equation 9) as

$$p_{\vartheta_{jl}}(t) = -\frac{1}{\omega} \frac{d\varphi(t)}{dt}. \tag{10}$$

Therefore, the use of Equation 9 corresponds to the widely used power law memory function, that is, $\varphi(t) = \omega \tau^\beta t^{-\beta}$ (Haggerty et al., 2000). The workflow associated with the algorithm proposed to evaluate BTCs of a partitioning tracer at a given cross section of the flow and transport domain is graphically sketched in Figure 1.

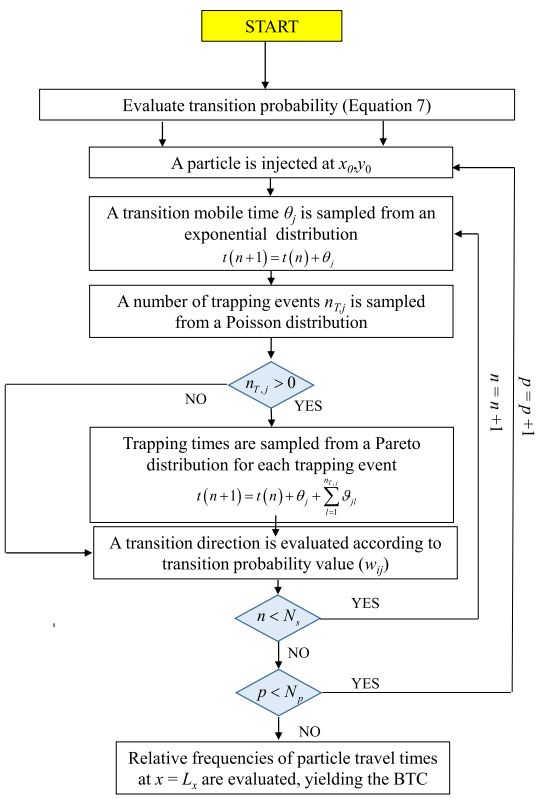

Figure 1. Sketch of the workflow associated with the algorithm proposed to evaluate BTCs of a partitioning tracer at a given cross section.

2.2. Model Calibration

Let N_c be the number of concentration data associated with tracer η in the water phase (w). These are collected in vector $\mathbf{c}^*_{\eta,w}$ (the symbol * is employed to denote experimental observations), that is, $\mathbf{c}^*_{\eta,w} = \left[c^*_{\eta,w_1}, c^*_{\eta,w_2}, ..., c^*_{\eta,w_{N_C}}\right]^T$. We introduce the vector of unknown TDRW model parameters $\mathbf{p} = \left[S_{or}, K_\eta, \omega, \beta, \tau\right]^T$ and the vector of model-based concentrations $\mathbf{c}_{\eta,w} = \left[c_{\eta,w_1}, c_{\eta,w_2}, ..., c_{\eta,w_{N_C}}\right]^T$. As commonly assumed (e.g., Carrera & Neuman, 1986; Carrera et al., 2005; Chavent, 2010; Poeter & Hill, 1997; Tarantola, 2005), we consider errors

associated with concentration measurements to be uncorrelated. This renders a diagonal covariance matrix of concentration measurement errors, nonzero entries being equal to the observation error variance, σ^2_{η,w_i} (with $i = 1, \ldots, N_C$). Following Tellinghuisen (2009) and Bianchi Janetti et al. (2012), we set $\sigma_{\eta,w_i} = \sigma_0 c^*_{\eta,w_i}$, where σ_0 is related to the accuracy of the experimental device. This is related to the observation that the standard deviation of concentration measurements is not constant and is proportional to the measured concentration. Estimates of model parameters can then be obtained by considering concentration data. The data set can also be complemented by additional information. Here, we embed in the analysis experimental information, K^*_η, on the partition coefficient K_η. These data are usually available on the basis of batch experiments and are affected by an observation error variance, σ^2_K. Note that K_η is included in the set of uncertain model parameters since batch experiments estimated values are not always representative of flow through conditions.

First, we determine Maximum Likelihood (ML) estimates of $\mathbf{p}$, σ^2_0, and σ^2_K (denoted as $\hat{\mathbf{p}}$, $\hat{\sigma}^2_0$, and $\hat{\sigma}^2_K$, respectively) by minimizing of the Negative Log Likelihood criterion (NLL)

$$\mathrm{NLL} = \frac{J}{\sigma^2_0} + N_C \ln \sigma^2_0 + \ln \sigma^2_K + 2 \sum_{i=1}^{N_C} \ln c^*_{\eta,w_i} + (N_C + 1)\ln 2\pi, \tag{11}$$

where

$$J = \left[\mathbf{c}^*_{\eta,w} - \mathbf{c}_{\eta,w}\right]^T \underline{\underline{\boldsymbol{\Sigma}}}^{-1} \left[\mathbf{c}^*_{\eta,w} - \mathbf{c}_{\eta,w}\right] + \lambda\left(K^*_\eta - K_\eta\right)^2 \text{ with } \lambda = \sigma^2_0/\sigma^2_K. \tag{12}$$

Here, $\underline{\underline{\boldsymbol{\Sigma}}}$ is a diagonal matrix of size $N_C \times N_C$ with entries $\Sigma_{ii} = \left(c^*_{\eta,w_i}\right)^2$ and λ serves as a weight of the regularization term associated with K^*_η. Note that on the basis of Equation 3 if no information on the partition coefficient is available (which corresponds to disregarding the regularization term in Equation 12), one cannot estimate jointly S_{or} and K_η but only the retardation factor. Hence, relying on available information about the partition coefficient (albeit typically stemming from batch tests) is critical to estimate both parameters.

Minimization of Equation 12 with respect to $\mathbf{p}$, σ^2_0, and σ^2_K is likely to be unstable (see Carrera & Neuman, 1986). Thus, we follow the procedure proposed by Carrera and Neuman (1986) and (a) fix the value of the regularization weight λ; (b) minimize J (Equation (12)) to obtain J_{min} and a ML estimate of $\mathbf{p}$, $\hat{\mathbf{p}}$; (c) compute a ML estimate of σ^2_0 as $\hat{\sigma}^2_0 = J_{min}/(N_c + 1)$; and (d) compute a ML estimate of σ^2_K as $\hat{\sigma}^2_K = \sigma^2_0/\lambda$. Steps (b)–(d) are repeated for several values of the λ until a minimum NLL (Equation 11) is identified. This procedure constitutes the backbone of the classical ML approach. It yields best estimates of model parameters and is here applied by considering the experimental observations provided by Dwarakanath et al. (1999).

Considering the classical ML approach, the constant σ^2_0 estimated at the end of the inversion as explained above includes both model and experimental errors. Assessing model error would require considering alternative interpretive models and rank them on the basis of various criteria, accounting for their quality of fit to observations and number of parameters (see, e.g., Bianchi Janetti et al., 2012). To this purpose, the experimental BTC of a partitioning tracer is interpreted according to the following alternative models: (a) the TDRW model proposed in the manuscript, (b) the advection dispersion equation with a linear retardation factor, and (c) the advection dispersion equation with a non-linear retardation factor (based on Langmuir isotherm). In Supporting Information S1, we show that the proposed TDRW model can be preferable to other models characterized by a reduced number of parameters on the basis of *AIC* and *BIC* criteria (Akaike, 1974; Schwartz, 1978).

Probability distributions of model parameters conditional on available data can then be evaluated through a stochastic inverse modeling approach. We do so by performing minimization of Equation 12 upon considering a collection of N_{MC} random realizations of the vector $\mathbf{c}^*_{\eta,w}$ and of K^*_η. These realizations are obtained by perturbation of $\mathbf{c}^*_{\eta,w}$ and K^*_η through Gaussian white noises whose variances are set to yield a given value of λ. The stochastic inversion is then repeated for various values of λ to assess the impact of the latter on the probabilistic distribution of uncertain model parameters. Note that the chosen Gaussian distribution for realizations of $\mathbf{c}^*_{\eta,w}$ and K^*_η is a typical choice and is based on the idea that measurement errors are accidental. This choice is at the basis of the ML approach and allows deriving Equations 11 and 12.

Minimization of Equation 12 is obtained through a standard genetic algorithm implemented in the MATLAB environment (i.e., the *ga* function of MATLAB R2021b). The latter enables an efficient search of the parameter space during model inversion. The algorithm starts by evaluating Equation 12 for an initial population of M

points in the parameter space. At each step, the minimization algorithm makes use of the selection, crossover, and mutation functions to randomly produce new individuals that are characterized by a decreased value of the objective function (i.e., of Equation 12). The algorithm converges after N iterations when a given population does not produce an offspring that is significantly different from any of the previous ones. This procedure requires performing $N_{MC} \times M \times N$ runs of the forward model. Note that the values of N_{MC}, M, and N need to be sufficiently high to ensure (a) stability in the computation of the parameter distributions as well as (b) convergence of the minimization algorithm.

It is remarked that relying on the full TDRW model set-up described in Section 2.1 to simulate tracer concentrations poses a significant challenge in terms of computational effort (see Section 3). For this reason, the target system response (i.e., a BTC associated with tracer concentration at specified times) is evaluated upon relying on a surrogate (or reduced-order) model. For the purpose of our study, a surrogate model based on the generalized Polynomial Chaos Expansion (gPCE; e.g., Le Maître & Knio, 2010; Porta et al., 2014; Xiu & Karniakidis, 2002) is considered, the presented methodology being fully compatible with other choices of model reduction techniques.

An additional advantage of employing a gPCE representation is that Sobol' indices (Sobol, 2001) can be computed with simple algebraic operations from the coefficients of the polynomial expansion. These indices are variance-based global sensitivity metrics and can be employed to apportion the variance of a target model output amongst the uncertain model parameters driving the system behavior. In this context, a global sensitivity analysis based on Sobol' indices is performed with the aim of diagnosing the model behavior across time by assessing the way uncertainty associated with model parameters affects uncertainty of the target modeling goals/results. With this spirit and consistent with the work of Dell'Oca et al. (2020), the sensitivity analysis is performed prior to model calibration. Details about the methodology employed to obtain the surrogate model approximation and the Sobol' sensitivity indices are illustrated in Appendix A. Note that our results should not be significantly affected by the choice of a different surrogate model characterized by a comparable error. This is related to the observation that we used the surrogate model solely to obtain a quick estimate of the target variable as a function of the uncertain model parameters to assist global sensitivity analysis and Sobol' indices evaluations. The accuracy of the adopted gPCE is assessed in Appendix A and in Supporting Information S1. We further note that in our case the need of the surrogate model was strictly related to the computational effort required for a single calibration with the full TDRW model. The reduction of time ensuing the use of a surrogate model with respect to the full model depends on many factors, such as, for example, the complexity of the full model, the number of parameters, or the order of regression. While reliance on a surrogate model unavoidably introduces an error, in some cases (as the one we consider) it is necessary to resort to it, given the computational time requirements to obtain stable and robust results.

3. Test Case and Experimental Data Set

The robustness of the proposed methodology and operational framework is assessed by considering the water-saturated column experiment performed at the laboratory scale and presented by Dwarakanath et al. (1999). The column is packed with alluvial aquifer material and residual DNAPL saturation, S_{or}, is attained via water-flooding. Injection of tracers is performed in the presence of a constant flow rate. A conservative (1-propanol) and four partitioning (1-pentanol, 3-methyl-3-pentanol, 2-ethyl-1-butanol and 1-hexanol) tracers characterized by diverse partitioning coefficients are simultaneously and instantaneously injected. Breakthrough curves are observed at the outlet section of the column.

The steady state mean flow is aligned along the x direction in the experimental setup (see Figure 2). We then model the system as a two-dimensional domain discretized into voxels of side $\Delta = 5 \times 10^{-4}$ m. This yields a lattice composed by 200×60 voxels along directions x and y, respectively (see Figure 2). Note that in this two-dimensional system, even as homogeneous, particles can migrate along two orthogonal directions. We chose to rely on such a conceptual picture to avoid further constraining of the modeling approach. Due to the imposed conditions, the velocity component along direction y vanishes. A constant dispersion coefficient $D = D_m + \alpha_L u$ is then considered, u, D_m, and α_L being the advective velocity along direction x, molecular diffusion, and longitudinal dispersivity, respectively. Simulation of the migration of each of the tracers considered is performed upon instantaneously injecting a set of $N_p = 10^6$ random walkers, uniformly distributed across the entire cross section of the domain at $x = 0$. A TDRW is then simulated for $N_s = 10^2$ time steps to obtain BTCs at the outlet (i.e., at $x = L_x$). Values of u and D are estimated by a classical ML model calibra-

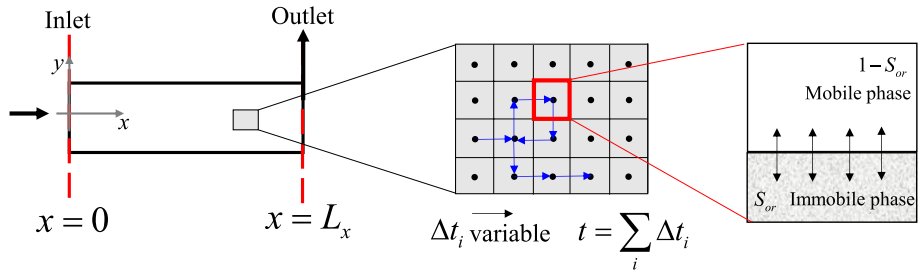

Figure 2. Geometry of the system and schematic representation of the TDRW modeling framework with trapping. Blue arrows in the central panel illustrate a particle trajectory for eight exemplary steps.

tion against the experimental BTC available for the conservative tracer. This yields $u = 1.4 \times 10^{-3}$ m s^{-1} and $D = 2.0 \times 10^{-6}$ m^2 s^{-1}. The corresponding Péclet number is $\mathrm{Pe} = uL_x/D = 70$. Model parameters $\mathbf{p}$ associated with a partitioning tracer are then estimated as detailed in Section 4. In principle, it would be possible estimating u and D together with $\mathbf{p}$. Otherwise, this would contribute to increase significantly the complexity of the calibration (also considering the limited amount of data available, see Section 4). Therefore, we follow a standard practice and rely on the analysis of conservative tracer data to infer values of u and D. Doing so enables us to gear our attention toward the calibration of the parameters associated with the partitioning tracer model, which is the focus of the work. The spatial discretization fulfills condition $\Delta < 2\,D/u$, to avoid numerical dispersion. Moreover, preliminary analyses have shown that the considered setting for N_p and Δ yields results that are not significantly affected by the number of particles and the spatial discretization (see in Supporting Information S1 for additional details) since these parameters mainly affect low concentration values for which no experimental data are available.

4. Results and Discussion

Application of the classical ML inversion considering the available experimental information yields ML estimates of σ_0^2, σ_K^2, and $\mathbf{p}$ for each of the partitioning tracers. Figure 3 depicts the Negative Log Likelihood (NLL) criterion evaluated after model inversion (conditional on the available data) versus $\lambda = \hat{\sigma}_0^2/\hat{\sigma}_K^2$ for the 1-pentanol partitioning tracer. NLL displays a minimum at $\lambda \approx 10^{-2}$. The ensuing model calibration results are listed in Table 2. For this value of λ, we obtain $\hat{\sigma}_0^2 = 0.0135$ and $\hat{\sigma}_K^2 = 1.35$. This result suggests that the estimated partition coefficient associated with the batch experiments is affected by an uncertainty which is significantly larger than that associated with the available concentration data since

$$\sigma_K^2 = \frac{\sigma_0^2}{\lambda} = \frac{\sigma_{\eta,w_i}^2}{\lambda c_{\eta,w_i}^2}, \qquad \text{i.e.,} \quad \frac{\sigma_K}{K_\eta} = a\frac{\sigma_{\eta,w_i}}{c_{\eta,w_i}} \qquad \text{with } a = \frac{c_{\eta,w_i}}{\sqrt{\lambda} c_{\eta,o_i}}. \tag{13}$$

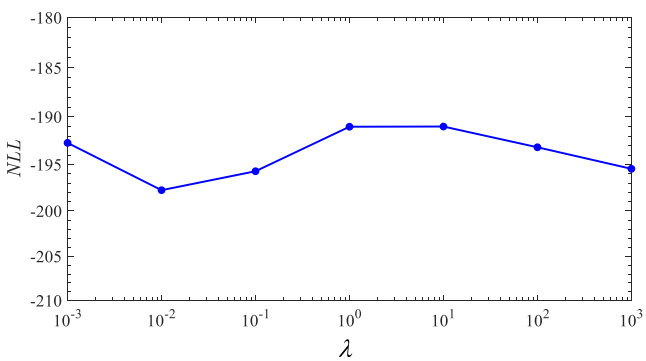

Figure 3. Dependence of NLL (Equation 11) on λ obtained through a classical ML model calibration conditional to the 1-pentanol partitioning tracer data.

We note that considering $\lambda \approx 10^{-2}$ and $\hat{K}_\eta = 4$ (see Table 2) yields $a \approx 2.5$ for the 1-pentanol tracer. This, in turn, leads to $\sigma_K/K_\eta < \sigma_{\eta,w}/c_{\eta,w}$.

It is further noted that our estimate of λ is consistent with the definition of K_η provided in Equation 2. This can be seen upon applying the formulation for error propagation to Equation 2, which in turn corresponds to a Taylor series expansion of σ_K^2 truncated at first order (under the assumption that $\sigma_{\eta,w}^2$ and $\sigma_{\eta,o}^2$ are sufficiently small) to obtain an approximate estimate of σ_K^2 as

$$\sigma_K^2 = \frac{1}{\overline{c}_{\eta,w}^2}\left(\sigma_{\eta,o}^2 + \frac{\overline{c}_{\eta,o}^2}{\overline{c}_{\eta,w}^2}\sigma_{\eta,w}^2\right). \tag{14}$$

Here, $\sigma_{\eta,w}^2$ and $\sigma_{\eta,o}^2$ are the variance of concentration measurements performed in the water and oil phase, respectively, in a batch system; the overbar denotes the mean operator and mean values of concentrations can be replaced by their experimental counterparts. Considering that $\sigma_{\eta,w}^2 = \sigma_0^2\overline{c}_{\eta,w}^2$ and $\sigma_{\eta,o}^2 = \sigma_0^2\overline{c}_{\eta,o}^2$ and substituting these expressions in Equation 14 yields

$$\sigma_K^2 = \frac{1}{\overline{c}_{\eta,w}^2}\left(\sigma_0^2\overline{c}_{\eta,o}^2 + \frac{\overline{c}_{\eta,o}^2}{\overline{c}_{\eta,w}^2}\sigma_0^2\overline{c}_{\eta,w}^2\right) = 2\sigma_0^2\frac{\overline{c}_{\eta,o}^2}{\overline{c}_{\eta,w}^2}. \quad (15)$$

From Equation 15 one can then note that $1/\lambda = 2\overline{c}_{\eta,o}^2/\overline{c}_{\eta,w}^2 = 2K_\eta^2$. Considering that $\hat{K}_\eta > 1$ for 1-pentanol (see Table 2), one can expect that $\lambda < 1$, which is consistent with our estimate.

Figure 4 depicts the temporal evolution of the concentrations of the conservative tracer (Propanol) and the four partitioning tracers (1-pentanol, 3-methyl-3-pentanol, 2-ethyl-1-butanol, and 1-hexanol). Symbols and curves correspond to experimental values and classical ML model calibration results, respectively. The BTCs are affected by increasingly significant retardation as $\hat{K}_\eta$ increases. As described by Equation 3, this corresponds to an increased effect of trapping of the partitioning tracer in the immobile phase. Figure 4 documents a very good agreement between numerical and experimental results for the range of investigated pore volumes (i.e., at all investigated times) and for all of the considered chemicals. While Dwarakanath et al. (1999) show that the partitioning tracer BTCs could not be interpreted through a classical advection dispersion model, our results document that the late time behavior of the BTCs is well interpreted by the TDRW model after a classical ML calibration. Note that our ML estimates $\hat{S}_{or}$ and $\hat{K}_\eta$ are consistent with the values reported by Dwarakanath et al. (1999), as seen by the results listed in Table 2 for all partitioning tracers. ML estimates of parameters characterizing the trapping phenomenon (i.e., $\hat{\omega}$, $\hat{\beta}$ and $\hat{\tau}$) are similar for all tracers. This result suggests that all of the investigated tracers are characterized by a similar behavior, as rendered through the analysis of the tail of the corresponding BTC.

Principal, $S_{p,i}$, and total, $S_{p,i}^T$, Sobol' indices associated with all (five) model parameters, $\mathbf{p}$, for the 1-pentanol tracer concentration are depicted in Figure 5. Sobol' indices are evaluated as a function of time (here expressed in terms of the injected pore volume) to detect the influence of each of the uncertain model parameters across various segments of the BTC. Our results show that the two parameters mainly affecting the variance of partitioning tracer concentration close to the peak (i.e., at PV $\approx$ 1.65) are K_η and S_{or}. This is related to the definition of retardation coefficient (see Equation 3) that directly embeds these two parameters. Considering the late time tails of the BTCs, suggests that the shape parameter of the distribution of the trapping times (i.e., β) governs the late time behavior of solute concentrations. Otherwise, with the exception of the early arrival times, Sobol' indices assign an almost negligible effect to parameters τ and ω, suggesting that the variance of partitioning tracer concentration is not significantly impacted by the number of trapping events.

Stochastic model calibration is then performed by relying on a collection of $N_{MC} = 1000$ realizations. These are obtained by perturbing experimental data as described in Section 2.2 and setting $M = 1000$. Calibration of each member of the ensemble involves running (on average) $N \approx 200$ model iterations. As indicated in Section 2.2, target system responses (e.g., tracer concentration at monitored times) are evaluated upon relying on surrogate models based on the generalized Polynomial Chaos Expansion (gPCE) to alleviate the computational effort. Note that the total CPU-time needed considering the gPCE approximation is ~2.0% of the one required upon relying on the full model (see Section 3). The assessment of the accuracy of the gPCE is described in Appendix A, where we show that the reduced model enables us to capture the full model results needed for the purpose of our analysis.

Figure 6 depicts normalized (with respect to the maximum concentration value) BTCs obtained for the collection of stochastic model calibrations upon setting λ = (a) 0.01, (b) 1.0, and (c) 100 for the 1-pentanol partitioning tracer. Gray curves correspond to the ensemble of TDRW results obtained upon minimizing Equation 12. The average BTC (continuous black curve) and the 95% confidence interval associated with the collection of stochastic inverse modeling results (demarcated by dashed black curves) are also shown. Red symbols represent the available experimental concentrations and their associated 95% confidence interval corresponding to $\pm 2\hat{\sigma}_0 c_{\eta,w_i}^*$ (where $\hat{\sigma}_0$ is evaluated through the ML model inversion, as described in Section 2.2). Most of the experimental concentration values lie inside the 95% confidence interval associated with inverse modeling results for all of the investigated values of λ. It can be noted that increasing the value of λ yields an enhanced spread of model results. It also yields a slightly worse (overall) match to the experimental data, as quantified in terms of the average (across the ensemble) value of J_{MIN}, which is equal to 0.798, 1.084, and 1.384 for $\lambda = 0.01$, 1 and 100, respectively. Average NLL values across the collection of inversions are equal to −178.11, −174.74, and −173.55 for $\lambda = 0.01$, 1, and 100, respectively. These results are consistent with those stemming from the classical ML inversion where a minimum NLL is observed at $\lambda = 0.01$ (see Figure 3).

Table 1
Selected Uncertain Model Parameters and Associated Intervals of Variability, as Defined by Their Lower (Min) and Upper (Max) Boundaries

Parameter	Description	Min	Max
S_{or}	Residual oil saturation	0.15	0.27
K_η	Partition coefficient	2.62	4.86
ω	Rate of trapping events	0.49	1.13
β	Shape parameter	0.50	1.10
τ	Scale parameter	6.10×10^{-4}	1.1×10^{-3}

As mentioned in Section 2.2, the regularization weight λ corresponds to the ratio between the variances of measurement errors associated with concentration and partition coefficient data. Thus, values of $\lambda < 1$ mimic experimental conditions where the error variance associated with the partition coefficient is higher than its counterpart related to solute concentrations, while $\lambda > 1$ corresponds to the opposite situation. For $\lambda = 100$ (see Figure 6c) any deviation of the estimated $\hat{K}_\eta$ value with respect to K_η^* has a marked weight in the objective function. Otherwise, setting $\lambda = 0.01$ (see Figure 6a) corresponds to imposing only a weak constraint on the estimated value of the partition coefficient. Note that, as hilighted in Section 2.2, the presence of the regularization term is key because it enables us to obtain joint estimates of the partition coefficient and of S_{or}.

Sample marginal distributions of estimated parameter values $\hat{\mathbf{p}}$ resulting from stochastic model calibration for the three investigated values of λ are depicted in Figure 7. These are complemented by sample distributions of the resulting retardation coefficient values obtained through Equation 3. As a reference, lower and upper limits of parameter supports listed in Table 1 and within which model inversion is performed are also depicted (vertical red lines). Parameter estimates ensuing the classical ML inversion based on available experimental data are also included (vertical black lines). These estimates approximately correspond to the most frequent value (i.e., the mode) of the sample distributions obtained with the stochastic inversions in most of the cases.

Sample distributions of $\hat{K}_\eta$ and $\hat{S}_{or}$ are significantly affected by λ. Their peak and standard deviation increase and decrease with λ, respectively. In particular, the uncertainty associated with the estimate of K_η is very low when $\lambda = 100$.

No clear trend with λ is detectable for the sample distributions of $\hat{\omega}$, $\hat{\beta}$, and $\hat{\tau}$. The distribution of $\hat{\omega}$ displays a bimodal character, with peaks that appear to increase with λ. The reduction of uncertainty due to ML inversion, with respect to initial parameter space bounds, is quite remarkable for parameter $\hat{\beta}$ while being less evident for $\hat{\omega}$ and $\hat{\tau}$, regardless of the value of λ. This result is consistent with the observation that the global sensitivity analysis reveals that ω and τ are not significantly affecting the target model output (see Figure 5). Conversely, note that all parameters are associated with distributions resulting from stochastic model calibration that are markedly different from the prior uniform density considered for the global sensitivity analysis before stochastic ML inversion.

Relationships between estimated parameter pairs can be visualized through scatterplots of parameter values obtained from the ensemble of N_{MC} inverse modeling results. As an example, Figure 8 depicts the scatterplot corresponding to the pair of estimated parameters $\hat{K}_\eta$-$\hat{S}_{or}$ for $\lambda = 0.01$, 1, and 100. The corresponding marginal distributions are also depicted together with parameter estimates obtained through the classical ML inversion based on available experimental data, for completeness. We note that $\hat{K}_\eta$ and $\hat{S}_{or}$ display a strong negative correlation for $\lambda = 0.01$ and 1. This is consistent with the way they appear in the definition of the retardation coefficient (see Equation 3). An empirical relationship between these two parameters can then be obtained, for example,

Table 2
Values of Model Parameter Estimates Obtained Through a Classical ML Inversion Considering the Available Experimental Information and $\lambda \approx 10^{-2}$

Parameter	Description	1-Pentanol	3-Methyl-3-pentanol	2-Ethyl-1-butanol	1-Hexanol
$\hat{S}_{or}$	Residual oil saturation	0.20	0.19	0.19	0.19
S_{or}^*	Residual oil saturation	0.18	0.18	0.18	0.18
$\hat{K}_\eta$	Partitioning coefficient	4.00	5.85	12.68	17.78
K_η^*	Partition coefficient	3.74	5.77	12.60	17.70
$\hat{\omega}$	Rate of trapping events	1.05	0.942	0.994	0.942
$\hat{\beta}$	Shape parameter	0.79	0.877	0.888	1.086
$\hat{\tau}$	Scale parameter	1.10×10^{-3}	1.00×10^{-3}	8.59×10^{-4}	1.10×10^{-3}

Note. *values reported by Dwarakanath et al. (1999).

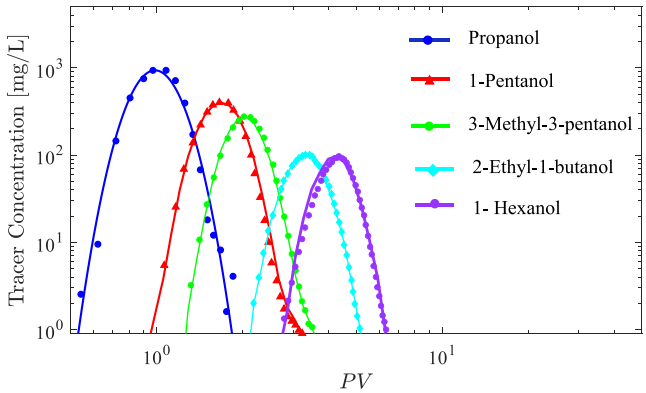

Figure 4. Experimental (symbols) and TDRW solution (curves) for the reference conservative tracer (propanol) and four partitioning tracers (1-pentanol, 3-methyl-3-pentanol, 2-ethyl-1-butanol, 1-hexanol) characterized by different partition coefficients. Parameters of the TDRW model are calibrated using a classical ML approach.

through a linear regression model. This yields $\hat{S}_{or} = -0.044\hat{K}_\eta + 0.38$ and $\hat{S}_{or} = -0.049\hat{K}_\eta + 0.40$ for $\lambda = 0.01$ and 1, respectively (with coefficient of determination $R^2 = 0.97$; see red lines in Figure 8). This result provides further support to the observation that information on the partition coefficient is critical for the joint estimation of K_η and S_{or}. Conversely, as mentioned above, for $\lambda = 100$ the estimate of the partition coefficient displays only a weak variability across realizations and is virtually uncorrelated with $\hat{S}_{or}$. It is noted that the width of the support of the sample distributions of the retardation coefficient ($\hat{R}_\eta$) resulting from stochastic model calibration increases with λ, with an ensuing decrease of the corresponding peak value (Figure 7f). Distributions of other pairs of parameters (including $\hat{\beta}$) are not characterized by significant correlation (not shown).

5. Conclusions

Our study provides a methodological framework for (a) the simulation of breakthrough curves (BTCs) associated with partitioning tracers observed in laboratory-scale column experiments and (b) a stochastic calibration of uncertain model parameters. The interpretive model is based on a TDRW particle tracking methodology to simulate solute transport through a porous medium. We extend the range of applicability of such an approach to include transport of partitioning tracers through the inclusion of retardation and trapping mechanisms. Model calibration is first performed through a classical Maximum Likelihood (ML) approach on the basis of experimental observations of chemical concentrations as well as information on the partition coefficient characterizing solute sorption. A stochastic inverse modeling approach is also employed to obtain sample probability distributions of model parameters conditional on available data. The applicability and the performance of the methodology are demonstrated upon considering the unique and extensive set of partitioning tracer experiments of Dwarakanath et al. (1999). Our work leads to the following major conclusions.

1. Comparisons between the experimental BTCs of Dwarakanath et al. (1999) and those stemming from classical ML calibration document the ability of a TDRW-based model tailored to simulate transport of partitioning tracers to characterize observed temporal histories of tracer concentration at the column outlet. This is seen across the whole range of investigated pore volumes (i.e., at all investigated times) and for all of the considered chemicals, characterized by different values of the partition coefficient, K_η.
2. Results from a global sensitivity analysis performed through classical Sobol' indices suggests that model parameters mainly affecting uncertainty of partitioning tracer concentration within the early/intermediate range of observation times (i.e., corresponding to a pore volume (PV) up to ≈2.0) are K_η and residual oil saturation, S_{or}. This is chiefly related to the definition of retardation coefficient that directly embeds these two parameters. Relying on a regularization term embedded in the Negative Log Likelihood criterion (NLL; Equations 11 and 12) enables us to include information on K_η in the context of ML model calibration. We show that considering these types of information, which are typically available on the basis of batch experiments, is critical to obtain joint estimates of K_η and S_{or}. Otherwise, late-time concentrations (i.e., corresponding to PV > 2.0) are mainly affected by the parameter β, characterizing the slope of the of the trapping time distribution.
3. Minimization of NLL for a classical ML model inversion (conditional on available data) is obtained for a values of the regularization weight $\lambda \approx 10^{-2}$. This suggests that the estimated partition coefficient associated with the batch experiments is affected by an uncertainty which is significantly larger than that associated with the available concentration data.

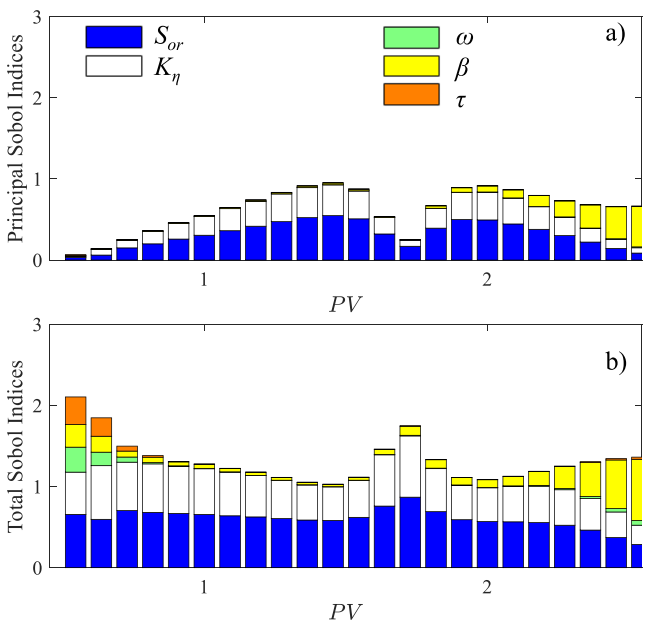

Figure 5. Principal and total Sobol indices associated with the five TDRW model parameters evaluated considering the 1-pentanol tracer concentration as target model output. The sensitivity indices are evaluated as a function of the pore volume.

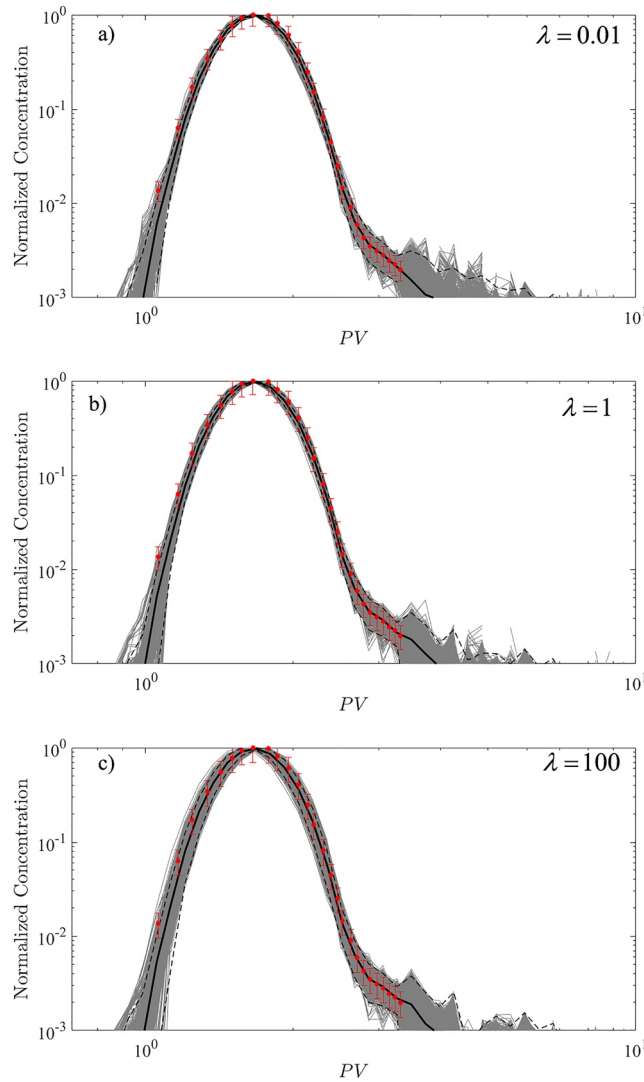

Figure 6. Collection of $N_{MC} = 1000$ breakthrough curves (continuous gray curves) obtained from the stochastic inverse modeling results considering λ = (a) 0.01, (b) 1, and (c) 100. Average (continuous black curve) and 95% confidence interval bounds (dashed black curves) are also shown. Red symbols correspond to available experimental concentrations. The associated 95% confidence intervals evaluated from a classical application of ML model calibration to the experimental data (see also Figure 4) is depicted (red vertical bars).

4. Model calibration performed in a stochastic context upon considering noisy data to mimic measurement errors associated with data collection yields sample probability distributions of model parameters conditional on available information. Considering the distributions of the estimated model parameters, we note that $\hat{K}_\eta$ and $\hat{S}_{or}$ display a strong negative correlation. This result provides additional support to the above mentioned observation that information on the partition coefficient, as guaranteed by the presence of a regularization term in the objective function, is important for the joint estimation of K_η and S_{or}.
5. Conditioning on available data through stochastic ML inversion yields a remarkable reduction of the uncertainty associated with some of the model parameters (i.e., $\hat{K}_\eta$, $\hat{S}_{or}$, and $\hat{\beta}$), with respect to the initial parameter space extent. The effect of conditioning on residual parameter uncertainty is less evident for the trapping rate, $\hat{\omega}$, and the scale parameter of the trapping time distribution, $\hat{\tau}$. The latter finding is consistent with the observation that the global sensitivity analysis reveals that ω and τ are not significantly affecting the target model output.

As a final remark, we note that a key feature of a stochastic model calibration approach is that the sample distribution of model parameters allows identifying a collection of possible model responses, fully conditional on a

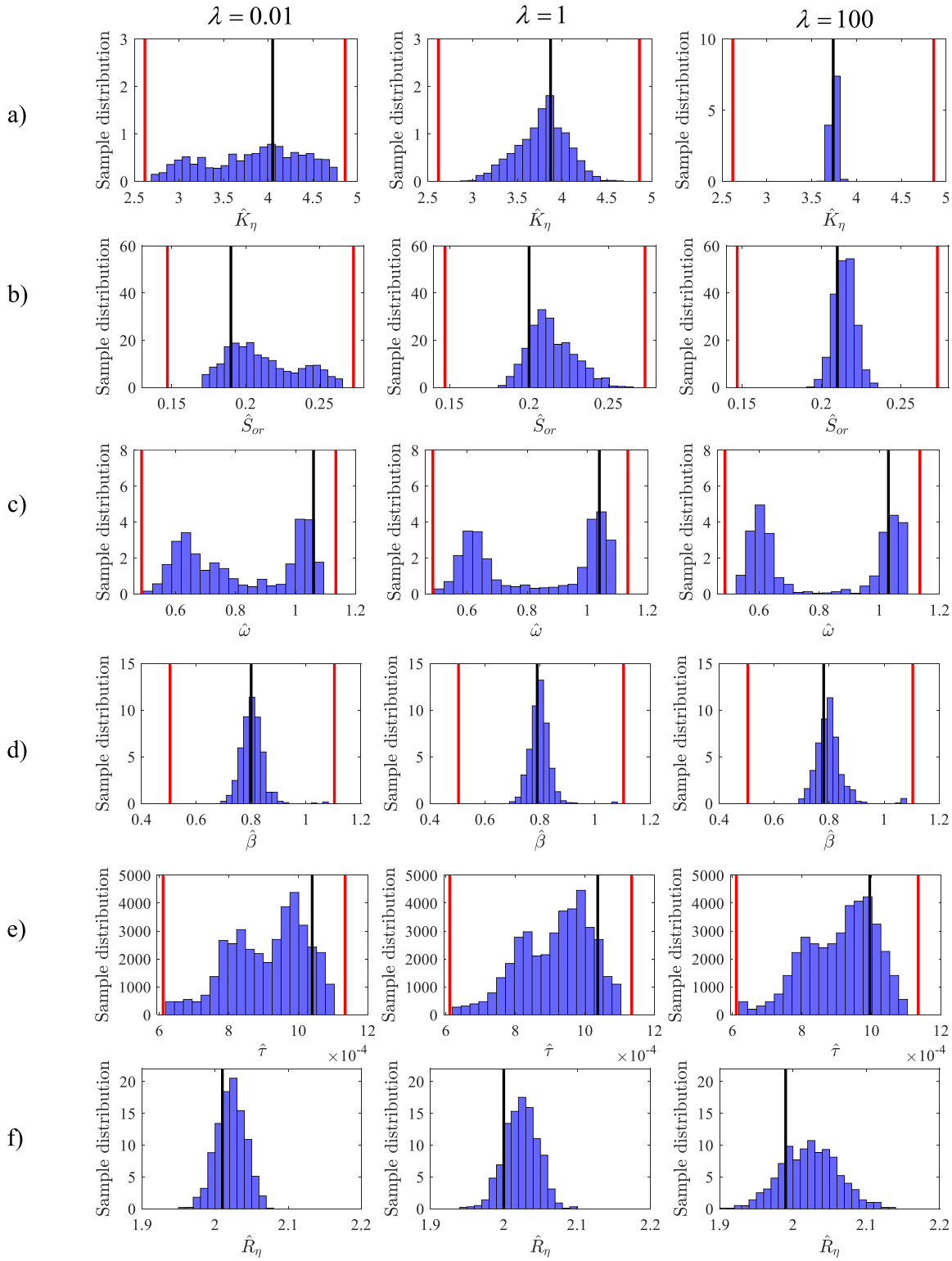

Figure 7. Sample marginal distributions of estimated parameter values resulting from stochastic model calibration for the three investigated values of λ: (a) $\hat{K}_\eta$, (b) $\hat{S}_{or}$, (c) $\hat{\omega}$, (d) $\hat{\beta}$, (e) $\hat{\tau}$. Sample distributions of the resulting retardation coefficient, $\hat{R}_\eta$, values obtained through Equation 3 are shown (f). Lower and upper limits of parameter supports within which model inversion is performed are also depicted (vertical red lines; see Table 1) together with parameter estimates obtained through the classical ML inversion based on available experimental data (vertical black lines).

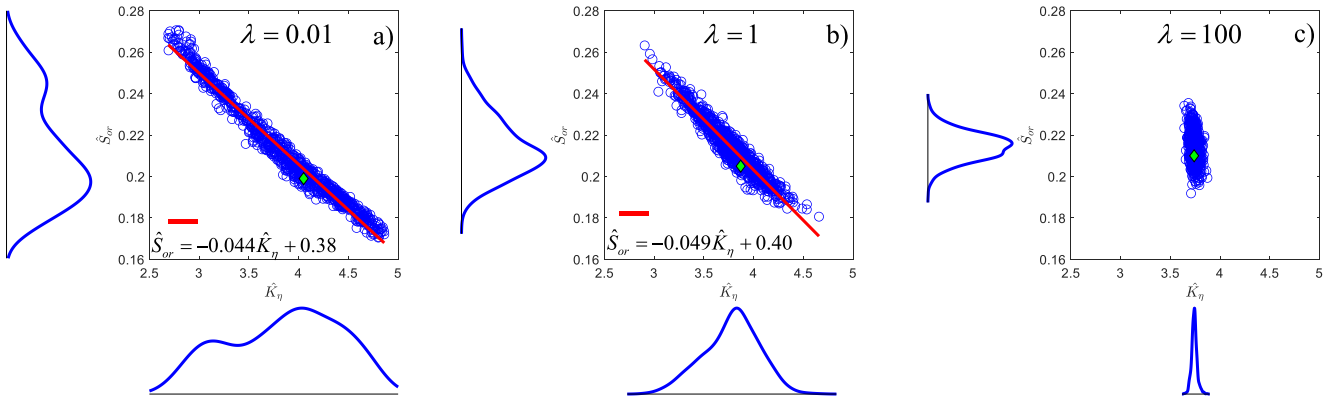

Figure 8. Scatterplots of pairs of $\hat{K}_\eta$-$\hat{S}_{or}$ values obtained from the ensemble of N_{MC} inverse modeling results for λ = (a) 0.01, (b) 1, and (c) 100. The corresponding marginal distributions are also depicted. A linear regression model is depicted in red for $\lambda = 0.01$ and 1. The green diamonds corresponds to parameter estimates obtained through the classical ML inversion based on available experimental data.

given set of observations of tracer concentration and model parameters. As such, this approach yields a collection of calibrated parameters which in principle could be used for stochastic simulation and characterization of scenarios of interest. In the current form, the methodology has been applied to model (section-averaged) breakthrough curves associated with homogeneous column tracer tests at the Darcy scale. It might be of interest to relate parameters governing a Darcy scale representation with descriptors associated with trapped phase ganglia distributions (e.g., their location and volume). This can certainly constitute a further development of our work, possibly in conjunction with detailed flow and transport experiments (eventually based on direct imaging) at various scales.

Appendix A: Surrogate Model and Sobol' Indices

The $M_P = 5$ uncertain parameters of the TDRW model are collected in a vector $\mathbf{p}$, that is, $\mathbf{p} = \left[S_{or}, K_\eta, \omega, \beta, \tau\right]^T$. For the purpose of evaluating the surrogate model, we consider the entries of $\mathbf{p}$ as independent and identically distributed (iid) random variables, each characterized by a uniform density. This enables us to assign equal weight to each of the values of a given model parameter within its support. The (random) parameter space across which the full system model is evaluated and the surrogate model is constructed is then defined as $\mathbf{\Gamma} = \left[\mathbf{p}^{\min}, \mathbf{p}^{\max}\right]$, $\mathbf{p}^{\min}$ and $\mathbf{p}^{\max}$ denoting vectors containing lower and upper bounds of parameter variability intervals, respectively (see Table 1). As stated in Section 2.2, our surrogate (or reduced-order) model relies on the generalized Polynomial Chaos Expansion, gPCE. We approximate $\mathbf{c}_{\eta,w}$ through a linear combination of multivariate orthonormal Legendre polynomials, that is, $\psi_{\boldsymbol{x}}(\boldsymbol{p})$, as

$$f(\boldsymbol{p}) \cong \gamma_{\mathbf{0}} + \sum_{i=1}^{M_P} \sum_{\boldsymbol{x}\in\mathfrak{I}_i} \gamma_{\boldsymbol{x}}\psi_{\boldsymbol{x}}(\boldsymbol{p}) + \sum_{i=1}^{M_P}\sum_{j>i}^{M_P} \sum_{\boldsymbol{x}\in\mathfrak{I}_{i,j}} \gamma_{\boldsymbol{x}}\psi_{\boldsymbol{x}}(\boldsymbol{p}) + \ldots;$$
$$\psi_{\boldsymbol{x}}(\boldsymbol{p}) = \prod_{i=1}^{M_P} \psi_{i,x_i}(p_i);\ \gamma_{\boldsymbol{x}} = \int_{\Gamma} f(\boldsymbol{p})\psi_{\boldsymbol{x}}(\boldsymbol{p})\rho_{\Gamma\boldsymbol{p}}\, d\boldsymbol{p}, \tag{A1}$$

where $\boldsymbol{x} = \{x_1, \ldots, x_M\} \in \mathbb{N}^{M_P}$ is a multi-index expressing the degree of each univariate polynomial, $\psi_{i,x_i}(p_i)$; $\gamma_{\boldsymbol{x}}$ are the gPCE coefficients; $\rho_{\Gamma\boldsymbol{p}}$ denotes the probability density of $\mathbf{p}$; $\mathfrak{I}_i$ and $\mathfrak{I}_{i,j}$ include all indices such that only the ith component does not vanish or only the ith and jth components are not zero, respectively, and so on. Evaluating coefficients $\gamma_{\boldsymbol{x}}$ in Equation A1 entails resorting to a regression-based method (Sudret, 2008). The latter is based on (a) the evaluation of the full model and its gPCE approximation at a number of points in the parameter space and (b) the minimization of the sum of the square of the differences between the exact and the approximated solutions. Here, accurate results have been obtained truncating the gPCE at order 5, considering $N_t = 2000$ full model runs. The latter are performed upon relying on a quasi-Monte Carlo sampling technique (see, e.g., Fajraoui et al., 2012; Maina & Guadagnini, 2018). The ability of a gPCE of a given order to approximate concentration at the target pore volumes (i.e., the N_s time steps encompassing the total temporal window analyzed in the TDRW simulations) is assessed upon considering the full model solutions evaluated at $N_V = 200$ sets of parameter values that are randomly selected

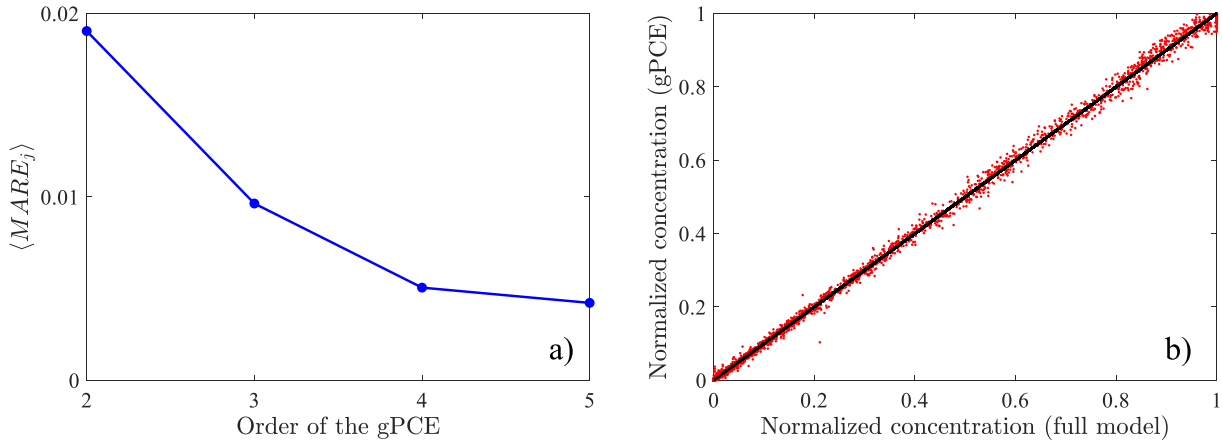

Figure A1. Performance of the surrogate model: (a) average $MARE_j$ metric (Equation A2) versus order of the generalized Polynomial Chaos Expansion (gPCE) approximation; (b) scatterplot of normalized solute concentration evaluated through the gPCE of order five versus their counterparts computed with the full model for the $N_V = 200$ sets of parameter values randomly selected in the parameter space and not employed for the assessment of the gPCE.

across the parameter space and are not employed for the assessment of the gPCE. For each target pore volume, we compute a mean absolute relative error ($MARE_j$) between the full model and the gPCE approximation, that is,

$$MARE_j = \frac{1}{N_V} \sum_{k=1}^{N_V} \frac{\left| c_{\eta,w_{j,k}} - c_{\eta,w_{gPCE,j,k}} \right|}{c_{\eta,w_{j,k}}} \quad j = 1, ..., N_s, \tag{A2}$$

where $c_{\eta,w_{j,k}}$ is concentration of the partitioning tracer η in the water phase evaluated with the full model at time step j with the set of parameters k, $c_{\eta,w_{gPCE,j,k}}$ is its counterpart computed with the gPCE.

Average values of $MARE_j$, denoted with $\langle MARE_j \rangle$ and evaluated for the set of the target pore volumes, are depicted in Figure A1a versus the order of gPCE approximation. $\langle MARE_j \rangle$ decreases with increasing order of the gPCE and is approximately equal to 0.4% when a gPCE at order five is adopted. Figure A1b depicts scatterplots of normalized (with respect to the maximum concentration value) concentrations evaluated with the full model and their counterparts evaluated with the gPCE approximation of order 5 for all N_V sets of parameter values. These results clearly denote a good agreement between full model results and the gPCE. They suggest that the considered surrogate model enables us to capture with high fidelity the full model results needed for the purpose of our analysis. Additional analyses on the accuracy of the proposed surrogate model are presented in Supporting Information S1.

Once the coefficients $\gamma_{\boldsymbol{x}}$ have been computed, approximations of the Sobol' indices can be obtained (see, e.g., Sudret, 2008 and references therein). First, we compute mean, E[f], and variance, V[f], of $f(\mathbf{p})$ as

$$\mathrm{E}[f] = \gamma_{\mathbf{0}}; \quad \mathrm{V}[f] = \sum_{\boldsymbol{x} \in \mathbb{N}^{M_P}} \gamma_{\boldsymbol{x}}^2 - \gamma_{\mathbf{0}}^2. \tag{A3}$$

Sobol' indices are then obtained as

$$S_{p_i} = \sum_{\boldsymbol{x} \in \mathfrak{I}_i} \frac{\gamma_{\boldsymbol{x}}^2}{\mathrm{V}[f]} \quad S_{p_{ij}} = \sum_{\boldsymbol{x} \in \mathfrak{I}_{i,j}} \frac{\gamma_{\boldsymbol{x}}^2}{\mathrm{V}[f]}. \tag{A4}$$

Here, S_{p_i} is the principal Sobol' index associated with the ith parameter and collects all contributions to the variance of $f(\mathbf{p})$ which are only due to the ith uncertain parameter, p_i; and $S_{p_{ij}}$ is the Sobol' index corresponding to the mixed effects of uncertain parameters p_i and p_j.

The total Sobol' index associated with p_i is then defined as

$$S_{p_i}^T = S_{p_i} + \sum_{i \neq j} S_{p_{i,j}} + \sum_{j,k \neq n} S_{p_{j,k,n}} + ... \tag{A5}$$

and includes the terms appearing in Equation A4 as well as all terms associated with the mixed effects of p_i and other random model parameters (e.g., the term $S_{p_{j,k,n}}$ includes the mixed effects of uncertain parameters p_j, p_k and p_n).

Data Availability Statement

The set of experimental observations of Dwarakanath et al. (1999) analysed in the manuscript, the breakthrough curves obtained with the TDRW particle tracking methodology considering the parameters estimated via classical Maximum Likelihood (ML) approach and the key results of the stochastic inverse modeling technique can be downloaded from Bianchi Janetti et al. (2023).

Acknowledgments
A. Guadagnini acknowledges funding from the European Union Next-GenerationEU (National Recovery and Resilience Plan – NRRP, Mission 4, Component 2, Investment 1.3 – D.D. 1243 2/8/2022, PE0000005) in the context of the RETURN Extended Partnership.

References

Akaike, H. (1974). A new look at the statistical model identification. *IEEE Transactions on Automatic Control*, *19*(6), 716–723. https://doi.org/10.1109/TAC.1974.1100705

Allison, S. B., Pope, G. A., & Sepehrnoori, K. (1991). Analysis of field tracers for reservoir description. *Journal of Petroleum Science and Engineering*, *5*(2), 173–186. https://doi.org/10.1016/0920-4105(91)90066-V

Annable, M. D., Rao, P. S. C., Hatfield, K., Graham, W. D., Wood, A. L., & Enfield, C. G. (1998). Partitioning tracers for measuring residual NAPL: Results from a field scale test. *Journal of Environmental Engineering*, *124*(6), 498–503. https://doi.org/10.1061/(asce)0733-9372(1998)124:6(498)

Banton, O., Delay, F., & Porel, G. (1997). A new time domain random walk method for solute transport in 1-D heterogeneous media. *Ground Water*, *35*(6), 1008–1013. https://doi.org/10.1111/j.1745-6584.1997.tb00173.x

Benson, D. A., & Meerschaert, M. M. (2009). A simple and efficient random walk solution of multi-rate mobile/immobile mass transport equations. *Advances in Water Resources*, *32*(4), 532–539. https://doi.org/10.1016/j.advwatres.2009.01.002

Bianchi Janetti, E., Guadagnini, A., & Riva, M. (2023). Posterior assessment of parameters in a time domain random walk model of partitioning tracer tests in two-phase flow scenarios [Dataset]. Mendeley Data. Retrieved from https://data.mendeley.com/datasets/42gc584b99/1

Bianchi Janetti, E., Dror, I., Riva, M., Guadagnini, A., & Berkowitz, B. (2012). Estimation of single-metal and competitive sorption isotherms through maximum likelihood and model quality criteria. *Soil Science Society of America Journal*, *76*(4), 1229–1245. https://doi.org/10.2136/sssaj2012.0010

Carrera, J., Alcolea, A., Medina, A., Hidalgo, J., & Slooten, L. J. (2005). Inverse problem in hydrogeology. *Hydrogeology Journal*, *13*(1), 206–222. https://doi.org/10.1007/s10040-004-0404-7

Carrera, J., & Neuman, S. P. (1986). Estimation of aquifer parameters under transient and steady state conditions:1. Maximum likelihood method incorporating prior information. *Water Resources Research*, *22*(2), 199–210. https://doi.org/10.1029/WR022i002p00199

Carrera, J., Sanchez-Vila, X., Benet, I., Medina, A., Galarza, G., & Guimera, J. (1998). On matrix diffusion, formulations, solutions methods and qualitative effects. *Hydrogeology Journal*, *6*(1), 178–190. https://doi.org/10.1007/s100400050143

Chavent, G. (2010). *Nonlinear least squares for inverse problems*. Springer.

Cvetkovic, V., Painter, S., Outters, N., & Selroos, J. O. (2004). Stochastic simulation of radionuclide migration in discretely fractured rock near the spö Hard Rock Laboratory. *Water Resources Research*, *40*(2), W02404. https://doi.org/10.1029/2003WR002655

Dean, R. M., Walker, D. L., Dwarakanath, V., Malik, T., Spilker, K., & Chevron, E. T. C. (2016). Use of partitioning tracers to estimate oil saturation distribution in heterogeneous reservoir. *SPE-179655-MS*. https://doi.org/10.2118/179655-MS

Delay, F., Ackerer, P., & Danquigny, C. (2005). Simulating solute transport in porous or fractured formations using random walk particle tracking: A review. *Vadose Zone Journal*, *4*(2), 360–379. https://doi.org/10.2136/vzj2004.0125

Delay, F., Porel, G., & Sardini, P. (2002). Modelling diffusion in a heterogeneous rock matrix with a time-domain Lagrangian method and an inversion procedure. *Geoscience*, *334*(13), 967–973. https://doi.org/10.1016/S1631-0713(02)01835-7

Dell'Oca, A., Riva, M., & Guadagnini, A. (2020). Global sensitivity analysis for multiple interpretive models with uncertain parameters. *Water Resources Research*, *56*(2), e2019WR02575. https://doi.org/10.1029/2019WR025754

Dentz, M., & Berkowitz, B. (2003). Transport behavior of a passive solute in continuous time random walks and multirate mass transfer. *Water Resources Research*, *39*(5), 1111. https://doi.org/10.1029/2001WR001163

Dentz, M., Gouze, P., Russian, A., Dweik, J., & Delay, F. (2012). Diffusion and trapping in heterogeneous media: An inhomogeneous continuous time random walk approach. *Advances in Water Resources*, *49*, 13–22. https://doi.org/10.1016/j.advwatres.2012.07.015

Dwarakanath, V., Deeds, N., & Pope, G. A. (1999). Analysis of partitioning interwell tracer tests. *Environmental Science & Technology*, *33*(21), 3829–3836. https://doi.org/10.1021/es990082v

Fajraoui, N., Mara, T. A., Younes, A., & Bouhlila, R. (2012). Reactive transport parameter estimation and global sensitivity analysis using sparse polynomial chaos expansion. *Water, Air & Soil Pollution*, *223*(7), 4183–4197. https://doi.org/10.1007/s11270-012-1183-8

Haggerty, R., & Gorelick, S. M. (1995). Multiple-rate mass transfer for modeling diffusion and surface reactions in media with pore-scale heterogeneity. *Water Resources Research*, *31*(10), 2383–2400. https://doi.org/10.1029/95WR10583

Haggerty, R., McKenna, S., & Meigs, L. C. (2000). On the late-time behaviour of tracer breakthrough curves. *Water Resources Research*, *12*, 3467–3479. https://doi.org/10.1029/2000WR900214

Huseby, O., Hartvig, S. K., Jevanord, K., & Dugstad, Ø. (2015). Assessing EOR Potential from partitioning tracer data. In *SPE Middle East oil & gas show and Conference*. Manama, Baharain. https://doi.org/10.2118/172808-MS

James, S. C., & Chrysikopoulos, C. V. (2001). An efficient particle tracking equation with a specified spatial step for the solution of the diffusion equation. *Chemical Engineering Science*, *56*(23), 6535–6543. https://doi.org/10.1016/S0009-2509(01)00344-X

Jin, M., Bultler, G. W., Jackson, R. E., Mariner, P. E., Pickens, J. F., Pope, G. A., et al. (1997). Sensitivity models and design protocol for partitioning tracer tests in alluvial aquifers. *Groundwater*, *35*(6), 964–972. https://doi.org/10.1111/j.1745-6584.1997.tb00168.x

Jin, M., Delshad, M., Dwarakanath, V., McKinney, D. C., Pope, G. A., Sepehrnoori, K., et al. (1995). Partitioning tracer test for detection, estimation and remediation performance assessment of subsurface nonaqueous phase liquids. *Water Resources Research*, *31*(5), 1201–1211. https://doi.org/10.1029/95WR00174

Kinzelbach, W. (1998). The random walk method in pollutant transport simulation. In *Groundwater flow and quality Modelling*.

Le Maître, O., & Knio, O. (2010). *Spectral methods for uncertainty quantification*. Scientific Computation, Springer. https://doi.org/10.1007/978-90-481-3520-2_1

Maina, F. Z., & Guadagnini, A. (2018). Uncertainty quantification and global sensitivity analysis of subsurface flow parameters to gravimetric variations during pumping tests in unconfined aquifers. *Water Resources Research*, *54*(1), 501–518. https://doi.org/10.1002/2017WR021655

Noetinger, B., & Estebenet, T. (2000). Up-scaling of double porosity fractured media using continuous-time random walks methods. *Transport in Porous Media*, *39*(3), 315–337. https://doi.org/10.1023/A:1006639025910

Painter, S., Cvetkovic, V., Mancillas, J., & Pensado, O. (2008). Time domain particle tracking methods for simulating transport with retention and first-order transformation. *Water Resources Research*, *44*(1), W01406. https://doi.org/10.1029/2007WR005944

Poeter, E. P., & Hill, M. C. (1997). Inverse models: A necessary next step in groundwater modeling. *Ground Water*, *35*(2), 250–260. https://doi.org/10.1111/j.1745-6584.1997.tb00082.x

Porta, G. M., Tamellini, L., Lever, V., & Riva, M. (2014). Inverse modeling of geochemical and mechanical compaction in sedimentary basins through Polynomial Chaos Expansion. *Water Resources Research*, *50*(12), 9414–9431. https://doi.org/10.1002/2014WR015838

Rizzo, C., Nakano, A., & de Barros, F. P. J. (2019). PAR^2: Parallel random walk particle tracking method for solute transport in porous media. *Computer Physics Communications*, *239*, 265–271. https://doi.org/10.17632/4pkhgx8wcb.1

Russian, A., Dentz, M., & Gouze, P. (2016). Time domain random walks for hydrodynamic transport in heterogeneous media. *Water Resources Research*, *52*(5), 3309–3323. https://doi.org/10.1002/2015WR018511

Salamon, P., Fernandez-Garcia, D., & Gomez-Hernandez, J. J. (2006). A review and numerical assessment of the random walk particle tracking method. *Journal of Contaminant Hydrology*, *87*(3564), 277–305. https://doi.org/10.1016/j.jconhyd.2006.05.005

Schwartz, G. (1978). Estimating the dimension of a model. *Annals of Statistics*, *6*(2), 461–464. https://doi.org/10.1214/aos/1176344136

Shen, T., Moghanloo, R. G., & Tian, W. (2017). Interpretation of interwell chemical tracer tests in layered heterogeneous reservoir with crossflow SPE-187400-MS. https://doi.org/10.2118/187400-MS

Sobol, I. M. (2001). Global sensitivity indices for nonlinear mathematical models and their Monte Carlo estimates. *Mathematics and Computer in Simulation*, *55*(1–3), 271–280. https://doi.org/10.1016/S0378-4754(00)00270-6

Solcova, O., Krystynik, P., Dytrych, P., Bumba, J., & Kastanek, F. (2022). Typical groundwater contamination in the vicinity of industrial brownfields and basic methods of their treatment. *Ecotoxicology and Environmental Safety*, *233*, 113325. https://doi.org/10.1016/j.ecoenv.2022.113325

Sole-Mari, G., Fernàndez-Garcia, D., Sanchez-Vila, X., & Bolster, D. (2020). Lagrangian modeling of mixing-limited reactive transport in porous media: Multirate interaction by ex-change with the mean. *Water Resources Research*, *56*(8), e2019WR026993. https://doi.org/10.1029/2019WR026993

Sudret, B. (2008). Global sensitivity analysis using polynomial chaos expansions. *Reliability Engineering & System Safety*, *93*(7), 964–979. https://doi.org/10.1016/j.ress.2007.04.002

Tang, J. S. (1992). Interwell tracer test to determine residual oil saturation to waterflood at Judy Creek BHL Pool. *Journal of Canadian Petroleum Technology*, *31*(8), 61. https://doi.org/10.2118/92-08-06

Tarantola, A. (2005). Inverse Problem theory and methods for model parameter estimation SIAM. https://doi.org/10.1137/1.9780898717921

Tellinghuisen, J. (2009). Variance function estimation by replicate analysis and generalized least squares: A Monte Carlo comparison. *Chemometrics and Intelligent Laboratory System*, *99*(2), 138–149. https://doi.org/10.1016/j.chemolab.2009.09.001

Xiu, D., & Karniakidis, G. E. (2002). The Wiener-Askey polynomial chaos for stochastic differential equations. *SIAM Journal on Scientific Computing*, *24*, 614–644. https://doi.org/10.1137/S1064827501387826

References From the Supporting Information

Bedekar, V., Morway, E. D., Langevin, C. D., & Tonkin, M. J. (2016). MT3D-USGS version 1: A U.S. Geological Survey release of MT3DMS updated with new and expanded transport capabilities for use with MODFLOW. https://doi.org/10.3133/tm6A53

Harbaugh, A. W. (2005). MODFLOW-2005. The U.S. Geological Survey modular ground water model – The ground-water flow process. *U.S. Geological Survey Techniques and Methods*, *6-A16*.

Neuman, S. P., & Wierenga, P. J. (2003). *A comprehensive strategy of hydrogeologic modeling and uncertainty analysis for nuclear facilities and sites. NUREG/CR-6805*. U.S. Nuclear Regulatory Commission.

Neuman, S. P. (2003). Maximum likelihood Bayesian averaging of uncertain model predictions. *Stochastic Environmental Research and Risk Assessment*, *17*(5), 291–305. https://doi.org/10.1007/s00477-003-0151-7

Neuman, S. P., Xue, L., Ye, M., & Lu, D. (2011). Bayesian analysis of data-worth considering model and parameter uncertainties. *Advances in Water Resources*, *36*, 75–85. https://doi.org/10.1016/j.advwatres.2011.02.007

Ye, M., Neuman, S. P., & Meyer, P. D. (2004). Maximum likelihood Bayesian averaging of spatial variability models in unsaturated fractured tuff. *Water Resources Research*, *40*(5), W05113. https://doi.org/10.1029/2003WR002557

Ye, M., Meyer, P. D., & Neuman, S. P. (2008). On model selection criteria in multimodel analysis. *Water Resources Research*, *44*(3), W03428. https://doi.org/10.1029/2008WR006803